Hindawi
International Journal of Photoenergy
Volume 2021, Article ID 1884293, 8 pages
https://doi.org/10.1155/2021/1884293

Research Article

Two-Step Facile Preparation of 2D MoS_2/ZnO Nanocomposite *p-n* Junctions with Enhanced Photoelectric Performance

Ali Aldalbahi,[1] **Zhen-Bo Wang**,[2] **Tansir Ahamad**,[1] **Saad M. Alshehri**,[1] **and Peter X. Feng**[3]

[1]*Department of Chemistry, College of Science, King Saud University, Riyadh 11451, Saudi Arabia*
[2]*MIIT Key Laboratory of Critical Materials Technology for New Energy Conversion and Storage, State Key Lab of Urban Water Resource and Environment, School of Chemistry and Chemical Engineering, Harbin Institute of Technology, Harbin 150001, China*
[3]*Department of Physics, University of Puerto Rico, San Juan, PR 00936-8377, USA*

Correspondence should be addressed to Ali Aldalbahi; aaldalbahi@ksu.edu.sa and Peter X. Feng; peter.feng@upr.edu

Received 29 April 2021; Revised 10 July 2021; Accepted 6 August 2021; Published 14 August 2021

Academic Editor: Michael D. Heagy

Both *p-n* and *n-p* heterojunctions of ZnO-MoS_2 have been fabricated in order to understand the performance of electron and hole transport properties in solar cells and a self-powered photodetector system. Atomically thin 2-dimensional (2D) MoS_2 was prepared by using a spin coating method with controlled process times, whereas ZnO nanowires were prepared by using a plasma sputtering deposition technique. The nanoscale morphologies, composites, and photoelectric properties of nanocomposites were examined using scanning electron microscopy, energy-dispersive X-ray spectroscopy, and micro-Raman scattering spectroscopy, respectively. 2D heteronanostructures have exhibited an enhanced performance as compared to single-material-based prototypes. In photovoltaic mode, *n-p* heterojunction of the ZnO-MoS_2-based prototype appears to have much better photoelectric conversion efficiency than that in the case with *p-n* junction, indicating highly effective hole transport properties of 2D MoS_2 materials. Both band broadening and band shift were observed. Furthermore, the bias, annealing, and synergistic effects on the generated photocurrents and the response times were evaluated. The newly designed prototype exhibits exceptional properties: a broadband spectral response, a high signal-to-noise ratio, and excellent stability.

1. Introduction

Atomically thin 2-dimensional (2D) molybdenum disulfide (MoS_2) materials have attracted tremendous attention due to their unique electronic, photoelectric, and photocatalytic properties and immense potential in the fields of sensor, environment purification, and solar energy conversion [1–6]. During the last 10 years, many excellent results on investigations of electronic device based on 2D MoS_2 were reported [7, 8]. For instance, Tulsani et al. recently demonstrated for the first time matrix-free deposition of 2D MoS_2 sheets as an efficient hole transport layer for solar cells [9]. Wang et al. developed an ultrasensitive and broadband MoS_2 photodetector driven by ferroelectrics [10]. Frisenda et al. and Nalwa reviewed recent progress, challenges, and perspectives on the 2D MoS_2-based devices, respectively [11, 12]. It was found that the intrinsic defects in 2D MoS_2 are one of the challenges that limit its wide applications [13–15]. For example, the MoS_2 monolayer can absorb only 5% of incident light as compared to that of the bulk material, which greatly limits its use in solar cells, photodetector (PD) devices, and photocatalysis [16]. In order to meet such application, development of hybrid or heteronanostructures of 2D materials has made it possible to create and enhance multifunctional properties. Several cross-coupled properties, which are weak in single-phase materials, can be realized in the design of novel engineered materials based on hybrid nanostructures including graphene-MoS_2 [17, 18], WS_2-MoS_2 [19, 20], MoS_2-Si [21, 22], and MoS_2-TiO_2 [23, 24].

Recent studies have focused on obtaining the optimal heterostructures where nanostructured ZnO has attracted much interest because they are abundant, have high stability, are of simple composition, and therefore are amenable to low temperature, low cost, and scalable processing methods [25]. ZnO with a wurtzite structure is naturally an *n*-type semiconductor because of deviation from stoichiometry due to the

presence of intrinsic defects such as O vacancies and Zn interstitials. Previous experiments already demonstrated that multilayer MoS_2-ZnO heteronanostructures could effectively increase the spectral absorption range and promote the separation and migration of carriers through the built-in electric fields, thereby improving the photoelectric response characteristics [14]. Several hybrid MoS_2-ZnO nanomaterial-based prototypes such as flexible photodetectors and gas sensors have also been reported [26, 27]. Based on this point, it is necessary to further study new heteronanostructures and heterojunctions in the MoS_2/ZnO that may have new valuable applications in solar cells and self-powered photodetectors.

In the present work, the peculiar heterostructures obtained by coupling ZnO nanowires (NW) and 2D MoS_2 nanosheets (NS) with either *n*-*p*-type or *p*-*n*-type heterojunction nanostructures have been fabricated, characterized, and used for the development of prototypes of solar cells and self-powered photodetectors. The purpose is to understand how different nanocompositions and heterostructures affect the electron and hole transport in order to achieve the improvement of light absorption and transfer efficiency of photogenerated carriers. A newly fabricated prototype operating in photovoltaic mode exhibited much better photoelectric properties as compared to the recently published work [16]. Fast response, high photoelectric conversion efficiency, super stable baseline, and excellent repeatability have been obtained. Moreover, various bias effects and annealing effects on the performance of the prototype have also been carefully investigated.

2. Preparation of ZnO/MoS_2 Nanocomposites

Nano-MoS_2 samples were prepared by using a simple spin coating technique with commercial atomically thin MoS_2 nanosheet (NS) dispersion in solvents (dissolved in ethanol solution with concentration of 1 mg/mL from XFNANO Materials Co. Ltd.). The thicknesses of the samples deposited by spin coating were a function of the solution viscosity, concentration, and rotation velocity as well as the number of spin coating runs. Before preparing the MoS_2 samples, ultrasonic cavitation was used for 2 hours to disperse 2D sheets in solvents and break agglomerates in order to have a distribution uniformity. Each spin coating run was for 20 s with a spin rate of 3000 min^{-1}. Multiple coatings were used to increase the number of 2D MoS_2 sheets on the surface of substrates (Si or ZnO).

A commercial undoped ZnO target (from MTI Company) was used in the plasma sputtering deposition chamber, and the obtained nanostructured ZnO shows intrinsic *n*-type conductivity with very high electron densities.

Nanocrystalline Mn-doped zinc oxide $Zn_{1-x}Mn_xO$ ($x = 0$ –0.10) nanoparticles (NP) were synthesized on either Si or MoS_2 substrates by using the sol-gel technique at low temperature where Mn^{2+} ions were substituted into Zn^{2+} sites in the ZnO lattice that was confirmed by micro-Raman spectroscopy and X-ray photoelectron spectroscopy techniques. Detailed descriptions of syntheses and characterizations of these *n*-type and *p*-type ZnO materials could be found in our several previous works [28–30].

After annealing for 2 hours at 800°C, the films were examined by using JEOL 6480LV scanning electron microscopes (SEM) equipped with energy-dispersive X-ray spectroscopy (EDX) capabilities. Micro-Raman scattering measurements were carried out by using a Jobin-Yvon T64000 Triple-mate system with the radiation of 514.5 nm from a coherent argon laser, and a liquid N_2 cooled charge-coupled device system was used to collect and process the scattered data. Then, heteronanostructure-based prototypes were fabricated and their photoelectric properties were characterized. The main advantages are that syntheses of ZnO-MoS_2 heteronanostructures in the present work were extremely easy, and fabrication of the prototype was simple and cost-effective, while an enhanced light to electric power conversion efficiencies of photovoltaic prototypes were achieved.

3. Results and Discussion

3.1. Characterization

3.1.1. SEM. Figure 1(a) shows a typical SEM image of the nanostructured ZnO sample before deposition of atomically thin MoS_2 sheets. The sample mainly consists of a large amount of ZnO NWs. The average length and diameter of each wire is 4 μm and 0.5 μm, respectively. An estimated thickness of the sample is around 1.0~1.5 μm. No precise thickness of the film could be obtained because NWs were heavily overlapped one another with random distributions, resulting in a high roughness of the surface. This is very different from a solid flat thin film. These materials were then used to be combined together with 2D MoS_2 sheets to form double layers (ZnO-MoS_2) of heteronanostructures as shown in Figure 1(b) where the MoS_2 layer was prepared for 6 spin coating runs on ZnO. As seen, besides ZnO nanowires (NWs), a spin coating procedure produced a MoS_2 membrane consisting of a large number of randomly orientated nanosheets. Each sheet consisted of the stacked MoS_2 atomic layers. The size of each continuous sheet varied from 2 to 4 μm in diameter. Sheets overlapping heavily depended on the number of spin coating runs. A rough, irregular, and clustered surface type was generated when the number of spin coating runs was increased. This arrangement of numerous randomly orientated MoS_2 tightly packed into nanostructured ZnO would naturally result in a particular electronic structure, which determined the material's photoelectric capabilities. It should be mentioned that prior to each spin coating, the layer would be dried with hot air for 5 min.

Figure 1(c) shows the SEM image of MoS_2. High flexibility of MoS_2 is clearly visible that might make it possible to fabricate high-performance flexible electronics. Interestingly, the atomically thin MoS_2 nanosheets shown in Figures 1(b) and 1(c) did not appear to be well transparent, whereas highly transparent 2D MoS_2 could be easily observed from an optical microscopy as shown in the Figure 1 inset. This difference was because low-energy electrons could traverse

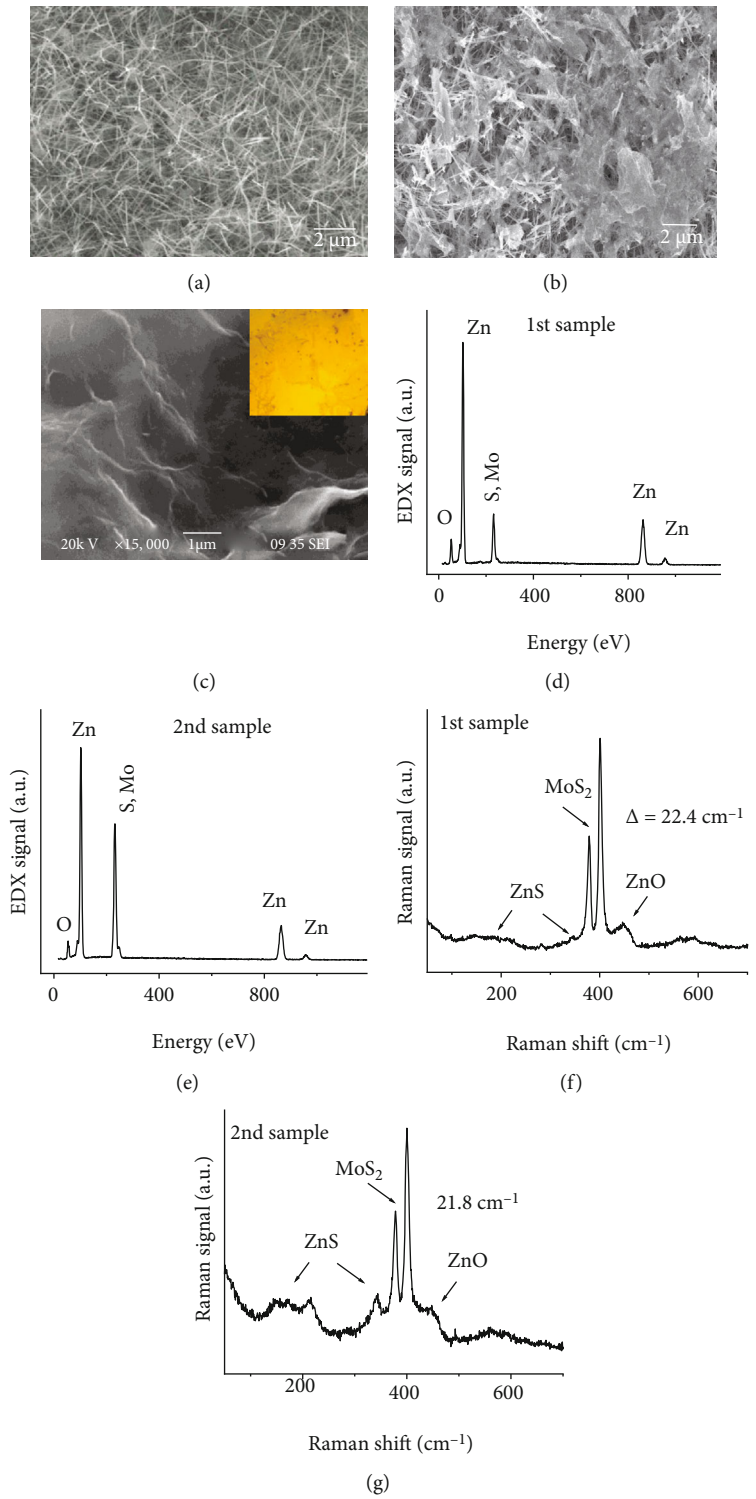

FIGURE 1: (a, b, c) Typical SEM images of nanostructured ZnO, ZnO-MoS_2, and MoS_2 samples; inset is an optical microscopy image of MoS_2. (d, e) EDX and (f, g) Raman scattering spectra of ZnO-MoS_2 where MoS_2 was prepared with 2 and 6 spin coating runs of deposition, respectively.

2D sheets, and the transparency of atomically thin MoS_2 can be visible only to electrons with energies less than 100 eV. However, electron energy in the present SEM is much larger than that of 100 eV.

3.1.2. EDX. The compositions of the samples were characterized using EDX. The results are shown in Figures 1(d) and 1(e) where the 1st sample and 2nd sample were prepared for 2 and 6 spin coating runs of MoS_2 on ZnO, respectively. As

seen, the relative ZnO EDX signal (Figure 1(d)) of the 1st sample was much stronger than that of the second sample (Figure 1(e)). In contrast, the MoS_2 EDX signal from the 1st sample was weaker than that of the 2nd one. This phenomenon could be attributed to different MoS_2 overlayer thicknesses prepared with different numbers of spin coating runs. The presence of S and Mo elements indicated the successful growth of the MoS_2. Element ratios between the S/Mo atoms remained almost unchanged, around 2, from the two samples. However, one would see from following Raman spectra that a new composite of ZnS resulting from chemical reaction suggested that a true ratio S/Mo in MoS_2 sheets would be slightly less than 2, indicating there were a little S vacancies in 2D samples that were associated with the *n*-type semiconductor behaviors. In contrast, *p*-type MoS_2 was fabricated by using a low-energy CH_4 plasma source to incorporate C dopants in MoS_2 semiconductors that were governed by kinetics.

3.1.3. Raman. Similar to EDX measurements, both samples were also analyzed by using Raman spectroscopy with a triple monochromator and a 514 nm Ar^+ ion laser beam, and the results are shown in Figures 1(f) and 1(g). Both Raman actives E^1_{2g} at 379.1 cm^{-1} and A_{1g} at 400.5 cm^{-1} modes were observed, indicating the MoS_2 phase. The extremely narrow Raman active E_{2g} peak indicated that the obtained MoS_2 has a low defect concentration. This is in good agreement with the data obtained by using EDX on quantitative analysis of the chemical composition where the ratio between the S and the Mo atoms remains nearly unchanged, close to 2. The wavenumber difference of 21.4 cm^{-1} between the E^1_{2g} and the A_{1g} peaks probably suggested that the average thickness of each sheet inside both samples was only two atomic layers. Detailed discussion of the relationship between the different shifts of Raman spectral lines and the MoS_2 atomic layers could be found in the previous work [12, 31].

ZnO Raman scattering spectral lines were also observed where the ZnO Raman signal (Figure 1(f)) from the 1st sample appears to be stronger than that (Figure 1(g)) from the 2nd sample. This is owing to the different abundances of MoS_2 sheets on the top overlayer. Low concentration of carbon impurity was detected, which was from the CH_4 plasma treatment for doping MoS_2.

Interestingly, Raman peaks associated with the chemical composite ZnS were also observed. Detailed description of ZnS Raman spectra could be found in the previous work [32]. Clearly, this component was from the interface where two types of materials in contact and chemical reaction to form a new composite would be further enhanced during annealing. As seen, the ZnS signal from the 2nd sample was lightly stronger than that of the 1st one, suggesting that this component increased with the increase in the number of spin coating runs. From the following experiments, it could be seen that 6 spin coating runs of deposition of 2D MoS_2 on ZnO would have better photoelectric conversion efficiency than that with the heterostructure prepared with 2 spin coating runs of deposition of 2D MoS_2 on ZnO. However, it is still not clear how much contribution was from the ZnS component.

3.2. Fabrications. In the present work, we extended the previous work on the use of a binary MoS_2 nanosheet semiconductor as an active layer by exploring emerging two types of composite heteronanostructures. The process flow of two types of fabrications is detailed in Figure 2. Both plasma puttering and spin coating techniques were utilized. For the first type of heteronanostructures, ZnO nanowires (NWs) were fabricated first by using sputtering and then spin coating was used to prepare 2D MoS_2 nanosheets (NS) on the surface ZnO NWs. In contrast, the 2nd type of the heteronanostructures was prepared only by the spin coating technique. The thickness of the generated sample depends on the number of spin coating runs.

3.3. Photoelectric Properties. Characterizations of photoelectric properties of the prototypes were performed on the homemade station. Detailed description of this station can be found from our previous work [33]. Briefly, two single calibrated LED light sources and a cheap commercial bulb light source were used, respectively, during the tests. Light illumination intensity was controlled by variation of the distance between the light source and the prototype. In the present case, the prototype was mounted at a fixed position, whereas the light source was removed to different positions away from the prototype so that the power densities of light illuminations on the surface of the active layer were controlled. Clearly, the light illumination intensity on the active layer decreased with the increase in the distance between the prototype and the light source.

Both samples were used for fabrications of two prototypes, respectively. Figure 3(a) shows responses of the 1st sample-based prototype exposed to a commercial white color bulb light illumination during cyclic tests with an 80-second period at room temperature (RT).

After the light source was turned on and off, the variation of the photocurrent was clearly visible. The generated photocurrent was directly associated with light absorption. The peak photocurrent up to 10 nA was obtained. In contrast, when the cyclic tests were performed on the 2nd prototype, better response with the improvement of response time and the signal-to-noise ratio was observed as shown in Figure 3(b). The obtained peak photocurrent was up to 12 nA. Clearly, high abundance of atomically thin MoS_2 sheets would yield benefits of more photocurrent generated. As seen, without any external power supply, the prototype exhibits a clean response, demonstrating that the ZnO-MoS_2 heteronanostructure-based prototypes are capable of photovoltaic mode operation.

However, strong noise was also observed. A tentative interpretation was that the noise probably came from light scattering in the bulb. Therefore, in the following experiments, the focus of the characterization would be on the 2nd sample-based prototype where two single wavelength collimated LED light sources ($\lambda = 750$ nm, 420 nm) would be used for tests.

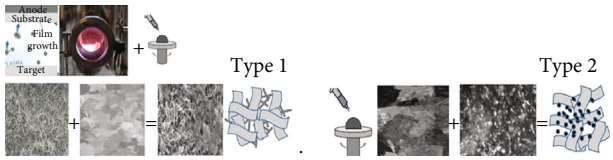

Figure 2: Process flow for two types of heteronanostructure fabrications.

Figure 4(a) shows typical responses of the *n*-ZnO NW/*p*-MoS_2 NS heteronanostructure-based prototypes operating in photovoltaic mode during cyclic tests. The data from cyclic tests clearly indicated that good repeatability and stable baseline features were achieved. As seen, the light-generated photocurrent rose rapidly at an initial period and then reached its maximum. Once the light source was turned off, the photocurrent quickly dropped. Since it operates in photovoltaic mode and does not require an external energy source, the obtained signals appeared to have very good signal-to-noise ratios and high stability, most likely due to the extremely low dark current or weak noise background.

The 420 nm light-generated photocurrent was up to $I_{ph, \lambda=420nm} = 120$ nA. As the distance between the prototype and the point shape of LED was 10 cm, the estimated intensity of the light illumination on the surface of the active layer was around 0.64 mW/cm^2 based on a spherical model. Accordingly, for the exposed area of ~9 mm^2 of the prototype, its responsivity is 2.1 mA/W. This value is almost 10 times larger than the recently reported results obtained from a similar ZnO-MoS_2 work [16]. Relatively, 750 nm light-generated photocurrent is only $I_{ph, \lambda=750nm} = 30$ nA, but response time and recovery time remained almost unchanged. In order to make a comparison, a binary MoS_2-based prototype was also fabricated and tested, and the results are shown in Figure 4(b). Two differences from the comparisons of the data shown in Figures 4(a) and 4(b) could be identified. (1) Light-generated photocurrent from the MoS_2-ZnO heteronanostructure-based prototype was clearly larger than that from the binary MoS_2-based prototype. (2) Photocurrent generated by blue light is larger than that generated by red light illumination in the MoS_2-ZnO heterostructure-based prototype, whereas in the MoS_2 system, the photocurrent generated by red light was larger than that yielded by blue light illumination even though the light illumination intensities remained unchanged. The band shift could be directly attributed to heterostructures.

Besides *n*-ZnO NW/*p*-MoS_2 NS-based prototype above, characterization of the 2nd type of heteronanostructures as the *n*-type MoS_2 NS/*p*-type ZnO nanoparticle- (NP-) based prototype as shown in Figure 2 was also carried out in order to understand different electron or hole transfer properties. The process of the fabrication of heterojunction was followed. Spin coating was used to have an atomically thin MoS_2 sheet-based film. Then, *p*-ZnO (Mn-doped ZnO) NP were prepared on the surface of MoS_2 to form *n*-MoS_2 NS/*p*-ZnO NP heterostructures. Basic characterization of its response to light illumination is shown in Figure 4(c). Good repeatability and stable baseline features were observed. However, very little photocurrent increases from *n*-MoS_2 NS/*p*-ZnO NP as compared to the result from the binary MoS_2-based prototype. This result probably indicated that 2D MoS_2 nanosheets are not an effective electron transport material in the solar cell system.

The comparison of the results from Figures 4(a) and 4(c) provided direct evidence on the difference of electronic transport in heterojunction even if one was based on ZnO nanowires and other was based on ZnO nanoparticles. In order to ensure the same conditions except for the doping type, additional experiments were also carried out where *p*-MoS_2 NS/*n*-type ZnO NP heterojunction was prepared and characterized, and results are shown in Figure 4(d). At the same density of blue light illumination, the generated photocurrent up to 70 nA was obtained. This value is almost 7 times larger than that with *n*-MoS_2 NS/*p*-ZnO NP. As seen, either the *n*-ZnO NW/*p*-MoS_2 NS- or *p*-MoS_2 NS/*n*-ZnO NP-based prototype appeared to have a good performance in the generated photocurrent and response time. Experimental data provided direct evidence on highly effective hole transport properties of 2D MoS_2 materials. However, the photocurrent strength would decrease with further increase in the film thickness in the *p*-MoS_2 NS/*n*-ZnO NP nanostructure. The optimal conditions for overlayer thickness, doping, and coping concentration still need to be further investigated, but one thing was clear that 2D heteronanostructures had exhibited an enhanced performance as compared to single-material-based devices.

3.4. Response Time. As expected, the prototype also had a good time response and time recovery. This is because the high quality of crystalline structure reduces the recombination and then reduces the response time. However, the real response speed was lower than they appeared. The results are shown in Figures 4(e) and 4(f), from which both response and recovery times were obtained around 20 and 60 ms, respectively. Much long response time and slight background shift with the bias applied were observed as reported by Wu et al. [16]. In the last part on discussing the bias effect, a slow response phenomenon would be further discussed. The main limit for the response time depends on the transit time of electrons and holes at the interfaces and junction among sheets in the prototype, the carrier diffusion, and the carrier multiplication process in the active layer, as well as the circuit time constant. It is expected that an atomically thin 2D sheet-based prototype should have a fast response speed, compared to samples composed of thick heteronanostructure. However, thick active layers exhibited much high photocurrent when exposed to light illumination. It was suggested that a fundamental trade-off between the photoconductive gain and the speed of a photodetector was unavoidable because a long minority carrier lifetime would result in photocurrent enhancement but increase the response time. Such behavior was very common but was not well understood due to the complex and multifactor nature. It could be believed, however, that the real recovery time of the sensor was lower than that appearing due to residual photoluminescence of the light source at the beginning of the on and off cycle.

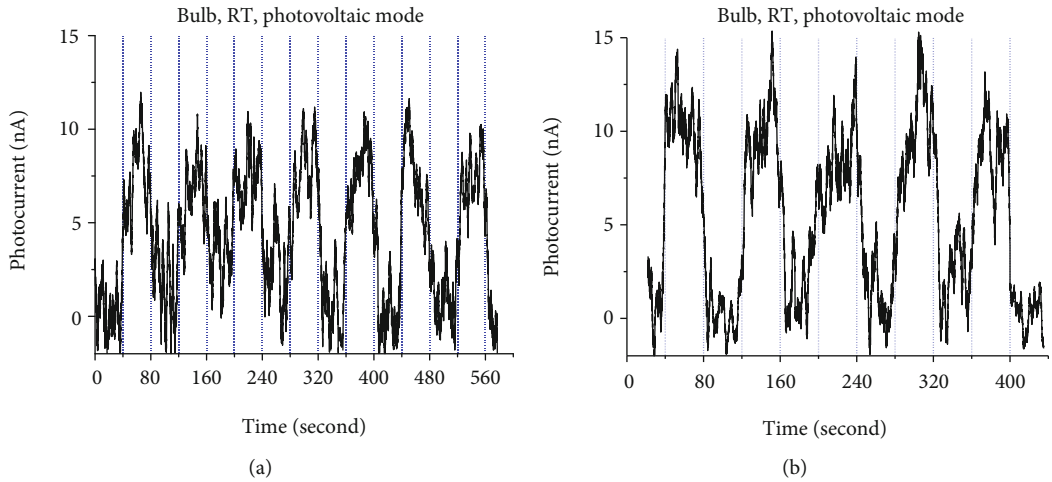

Figure 3: Responses of (a) 1st and (b) 2nd n-ZnO NW/p-MoS_2 NS-based prototypes exposed to commercial bulb light illuminations, respectively, during cyclic tests with 80 s period at room temperature (RT) and photovoltaic mode.

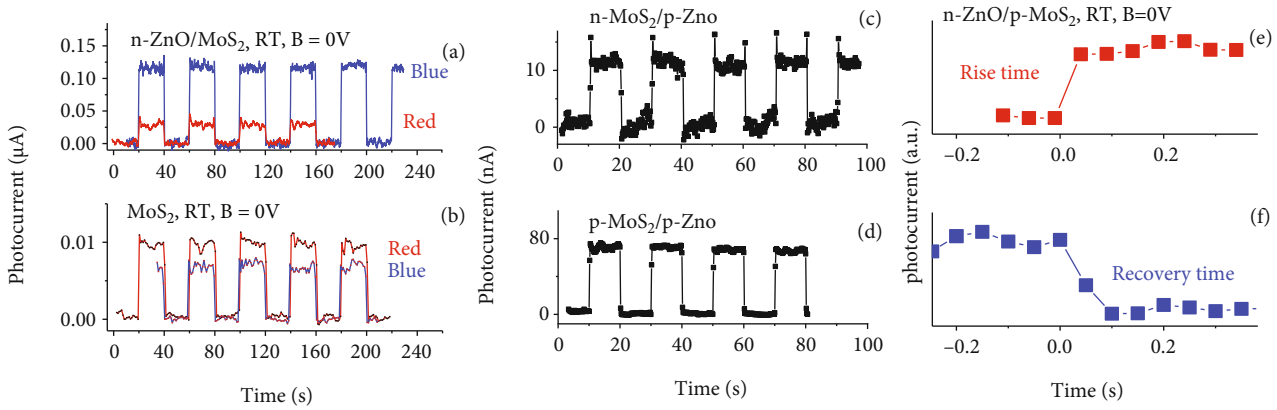

Figure 4: Responses of (a) n-ZnO NW/p-MoS_2 NS-based, (b) n-MoS_2 NS-based, (c) n-MoS_2 NS/p-ZnO NP-based, and (d) p-MoS_2 NS/n-ZnO NP-based prototypes exposed to light illuminations during cyclic tests in photovoltaic mode and at room temperature. (e, f) Response time and recovery time.

3.5. Bias Effect. Bias effect on the generated photocurrent was also studied. Similar to the experimental data shown in Figure 4(a), the prototype has a higher response strength to blue light illumination than that to red light illuminations at different bias applied as shown in Figure 5(a). Slight increase in bias voltage resulted in a great increase in photocurrent. As seen at the applied bias of 1 V, the 0.64 mW/cm^2 420 nm illumination yielded a photocurrent up to 7.8 μA, almost 65 times larger than that operated in photovoltaic mode. In contrast, 750 nm illumination generated the photocurrent around 5.2 μA. The prototype has a very broadband spectral response.

In order to understand the relations between the bias amplitude and the generated photocurrent, additional experiments were also carried out. Figure 5(b) shows the generated photocurrent of the prototype as a function of bias voltages. The inserts show the corresponding time-dependent responses at selected biases. High bias voltage yielded a high photocurrent or a large response rate (the ratio between the photocurrent output and the light illumination power input). As seen from Figure 5(b), the generated photocurrent at bias of 2 V is about 7 times as large as that at bias voltage of 0.5 V and about 200 times as large as that without a bias applied.

A large photoconductive gain is one of the main features for photoconductors. Their limitations include relatively large dark current (because of applied bias voltage). Therefore, the signal-to-noise ratio is relatively low. Large difference in response time was also observed. Both response time and recovery time are up to few seconds. A fundamental trade-off between the photoconductive gain and the speed is expectable. In order to effectively minimize this trade-off and to have a desirable balance between the sensitivity and the response time, zero bias in the present case would be preferable for high-performance devices.

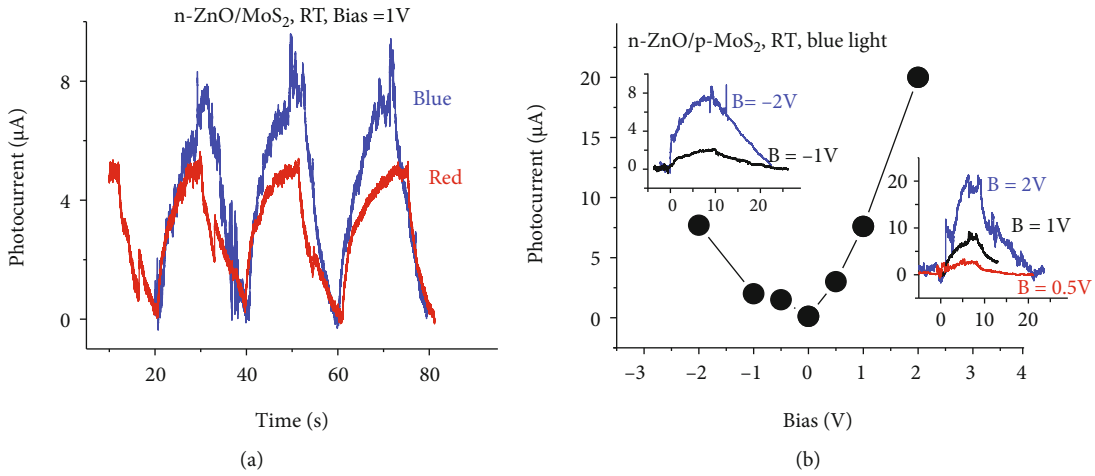

Figure 5: (a) Effect of bias on the responses of the *n*-ZnO NW/*p*-MoS_2 NS-based prototype exposed to 420 nm and 750 nm light illuminations, respectively. (b) The generated photocurrent as a function of applied bias.

4. Conclusions

Even though the methods used in preparations of nanocomposite materials were easy and fabrications of both *p-n* and *n-p* heterojunctions of ZnO-MoS_2 were simple and cost-effective, experiments demonstrated that the newly fabricated prototypes had very good performances including fast response time, high photocurrent, good baseline stability, and repeatability. Due to the extremely low dark current or weak noise background in photovoltaic mode operation, the prototype appeared to have an excellent signal-to-noise ratio. Maximum responsivity in photovoltaic mode operation up 2.1 mA/W and the response and recovery time less than 20 ms were obtained. From the comparisons of experiments, it was found that *n-p* heterojunction of the ZnO-MoS_2-based prototype has much better photoelectric conversion efficiency than that in the case of the *p-n* junction. Experimental data also provided direct evidence that 2D MoS_2 materials had highly effective hole transport properties.

The bias effect on the generated photocurrent was also studied. Slight increase in bias would result in a great increase in photocurrent. The main limitations were on its relatively large dark current and a slow response speed. A fundamental trade-off between the photoconductive gain and the speed of a photodetector was found. In order to effectively minimize this trade-off and to have a desirable balance between the response strength and the response time, a photoconductive mode of operation would be preferable for high-performance devices.

Data Availability

The data used to support the findings of this study are available from the corresponding author upon request.

Conflicts of Interest

There is no conflict of interest to declare.

Authors' Contributions

All authors work together on designing and performing the experiments, as well as analyzing the data and writing the manuscript.

Acknowledgments

This project was funded by the National Plan for Science, Technology and Innovation (MAARIFAH), King Abdulaziz City for Science and Technology, Kingdom of Saudi Arabia (Award Number 14-ENE1986-02).

References

[1] T. Pham, G. Li, E. Bekyarova, M. E. Itkis, and A. Mulchandani, "MoS_2-based optoelectronic gas sensor with sub-parts-per-billion limit of NO_2 gas detection," *ACS Nano*, vol. 13, no. 3, pp. 3196–3205, 2019.

[2] S. Rashidi, A. Caringula, A. Nguyen, I. Obi, C. Obi, and W. Wei, "Recent progress in MoS_2 for solar energy conversion applications," *Frontiers in Energy*, vol. 13, no. 2, pp. 251–268, 2019.

[3] K. Kumar, A. Kumar, and D. Kaur, "Improved power conversion efficiency in n-MoS_2/AlN/p-Si (SIS) heterojunction based solar cells," *Materials Letters*, vol. 277, p. 128360, 2020.

[4] V. Hasija, P. Raizada, V. K. Thakur, A. A. Parwaz Khan, A. M. Asiri, and P. Singh, "An overview of strategies for enhancement in photocatalytic oxidative ability of MoS_2 for water purification," *Journal of Environmental Chemical Engineering*, vol. 8, no. 5, p. 104307, 2020.

[5] Z. Wang and B. Mi, "Environmental applications of 2D molybdenum disulfide (MoS_2) nanosheets," *Environmental Science & Technology*, vol. 51, no. 15, pp. 8229–8244, 2017.

[6] R. Kumar, W. Zheng, X. Liu, J. Zhang, and M. Kumar, "MoS_2-based nanomaterials for room-temperature gas sensors," *Advanced Materials Technologies*, vol. 5, no. 5, article 1901062, 2020.

[7] E. Singh, P. Singh, K. S. Kim, G. Y. Yeom, and H. S. Nalwa, "Flexible molybdenum disulfide (MoS_2) atomic layers for

wearable electronics and optoelectronics," *ACS Applied Materials & Interfaces*, vol. 11, no. 12, pp. 11061–11105, 2019.

[8] D. Lembke, S. Bertolazzi, and A. Kis, "Single-layer MoS_2 electronics," *Accounts of Chemical Research*, vol. 48, no. 1, pp. 100–110, 2015.

[9] S. R. Tulsani, A. K. Rath, and D. J. Late, "2D-MoS_2 nanosheets as effective hole transport materials for colloidal PbS quantum dot solar cells," *Nanoscale Advances*, vol. 1, no. 4, pp. 1387–1394, 2019.

[10] X. Wang, P. Wang, J. Wang et al., "Ultrasensitive and broadband MoS_2 photodetector driven by ferroelectrics," *Advanced Materials*, vol. 27, no. 42, pp. 6575–6581, 2015.

[11] R. Frisenda, A. J. Molina-Mendoza, T. Mueller, A. Castellanos-Gomez, and H. S. J. Van Der Zant, "Atomically thin p-n junctions based on two-dimensional materials," *Chemical Society Reviews*, vol. 47, no. 9, pp. 3339–3358, 2018.

[12] H. S. Nalwa, "A review of molybdenum disulfide (MoS_2) based photodetectors: from ultra-broadband, self-powered to flexible devices," *RSC Advances*, vol. 10, no. 51, pp. 30529–30602, 2020.

[13] Y. Liu, Y. X. Yu, and W. De Zhang, "MoS_2/CdS heterojunction with high photoelectrochemical activity for H_2 evolution under visible light: the role of MoS_2," *Journal of Physical Chemistry C*, vol. 117, no. 25, pp. 12949–12957, 2013.

[14] Y. H. Tan, K. Yu, J. Z. Li, H. Fu, and Z. Q. Zhu, "MoS_2@ZnO nano-heterojunctions with enhanced photocatalysis and field emission properties," *Journal of Applied Physics*, vol. 116, no. 6, article 064305, 2014.

[15] W. Zhou, Z. Yin, Y. Du et al., "Synthesis of few-layer MoS_2 nanosheet-coated TiO_2 nanobelt heterostructures for enhanced photocatalytic activities," *Small*, vol. 9, no. 1, pp. 140–147, 2013.

[16] H. Wu, H. Jile, Z. Chen et al., "Fabrication of ZnO@MoS2 nanocomposite heterojunction arrays and their photoelectric properties," *Micromachines*, vol. 11, no. 2, p. 189, 2020.

[17] E. Lee, S. G. Lee, W. H. Lee et al., "Direct CVD growth of a graphene/MoS_2 heterostructure with interfacial bonding for two-dimensional electronics," *Chemistry of Materials*, vol. 32, no. 11, pp. 4544–4552, 2020.

[18] L. Yu, Y. H. Lee, X. Ling et al., "Graphene/MoS_2 hybrid technology for large-scale two-dimensional electronics," *Nano Letters*, vol. 14, no. 6, pp. 3055–3063, 2014.

[19] Y. Zhao, J. Liu, X. Zhang et al., "Convenient synthesis of WS_2–MoS_2 heterostructures with enhanced photocatalytic performance," *Journal of Physical Chemistry C*, vol. 123, no. 45, pp. 27363–27368, 2019.

[20] M. Morant-Giner, I. Brotons-Alcázar, N. Y. Shmelev et al., "WS2/MoS2 heterostructures through thermal treatment of MoS2 layers electrostatically functionalized with W3S4 molecular clusters," *Chemistry – A European Journal*, vol. 26, no. 29, pp. 6670–6678, 2020.

[21] A. Bablich, D. S. Schneider, P. Kienitz et al., "Few-layer MoS_2/a-Si:H heterojunction pin-photodiodes for extended infrared detection," *ACS Photonics*, vol. 6, no. 6, pp. 1372–1378, 2019.

[22] A. Hasani, Q. Van Le, M. Tekalgne et al., "Direct synthesis of two-dimensional MoS_2 on *p*-type Si and application to solar hydrogen production," *NPG Asia Materials*, vol. 11, no. 1, pp. 1–9, 2019.

[23] H. Liu, Y. Li, M. Xiang, H. Zeng, and X. Shao, "Single-layered MoS_2 directly grown on rutile TiO_2(110) for enhanced interfacial charge transfer," *ACS Nano*, vol. 13, no. 5, pp. 6083–6089, 2019.

[24] D. Wang, J. Li, A. Zheng et al., "Quasi-single-layer MoS_2 on MoS_2/TiO_2 nanoparticles for anthracene hydrogenation," *ACS Applied Nano Materials*, vol. 2, no. 8, pp. 5096–5107, 2019.

[25] R. L. Z. Hoye, K. P. Musselman, and J. L. Macmanus-Driscoll, "Research update: doping ZnO and TiO_2 for solar cells," *APL Materials*, vol. 1, no. 6, article 060701, 2013.

[26] M. A. Kang, S. Kim, I. S. Jeon et al., "Highly efficient and flexible photodetector based on MoS_2–ZnO heterostructures," *RSC Advances*, vol. 9, no. 34, pp. 19707–19711, 2019.

[27] S. Wang, W. Chen, J. Li, Z. Song, H. Zhang, and W. Zeng, "Low working temperature of ZnO-MoS_2 nanocomposites for delaying aging with good acetylene gas-sensing properties," *Nanomaterials*, vol. 10, no. 10, p. 1902, 2020.

[28] B. Yang, A. Kumar, P. Feng, and R. S. Katiyar, "Structural degradation and optical property of nanocrystalline ZnO films grown on Si (100)," *Applied Physics Letters*, vol. 92, no. 23, p. 233112, 2008.

[29] A. K. Singh, G. S. Thool, P. R. Bangal, S. S. Madhavendra, and S. P. Singh, "Low temperature Mn doped ZnO nanorod array: synthesis and its photoluminescence behavior," *Industrial and Engineering Chemistry Research*, vol. 53, no. 22, pp. 9383–9390, 2014.

[30] A. S. Ismail, M. H. Mamat, N. D. Md Sin et al., "Structural and optical properties of N-doped ZnO nanorod arrays prepared using sol-gel immersion method," in *2016 IEEE Student Conference on Research and Development (SCOReD)*, Kuala Lumpur, Malaysia, 2017.

[31] Y. Liu, H. Nan, X. Wu et al., "Layer-by-layer thinning of MoS_2 by plasma," *ACS Nano*, vol. 7, no. 5, pp. 4202–4209, 2013.

[32] J. Trajić, R. Kostić, N. Romčević et al., "Raman spectroscopy of ZnS quantum dots," *Journal of Alloys and Compounds*, vol. 637, pp. 401–406, 2015.

[33] P. X. Feng and A. Aldalbahi, "A compact design of a characterization station for far UV photodetectors," *The Review of Scientific Instruments*, vol. 89, no. 1, article 015001, 2018.